Real-time dual-wavelength digital holographic microscopy with a single hologram acquisition

Jonas Kühn[a], Tristan Colomb[b], Frédéric Montfort[c], Florian Charrière[a], Yves Emery[c], Etienne Cuche[c], Pierre Marquet[b] and Christian Depeursinge[a]

[a]*Ecole polytechnique fédérale de Lausanne, Institute of imaging and applied optics, CH-1015 Lausanne, Switzerland*

jonas.kuehn@a3.epfl.ch

http://apl.epfl.ch/page12232.html

[b]*Centre de Neurosciences Psychiatriques, Département de psychiatrie DP-CHUV, Site de Cery, 1008 Prilly-Lausanne, Switzerland*

[c]*Lyncée Tec SA, PSE-A, CH-1015 Lausanne, Switzerland*

http://www.lynceetec.com

Abstract: A technique to perform two-wavelengths digital holographic microscopy (DHM) measurements with a single hologram acquisition is presented. The vertical measurement range without phase ambiguity is extended to the micron-range, thanks to the resulting synthetic wavelength defined by the beating of two wavelengths with a separation of about 80nm. Real-time dual-wavelength imaging is made possible by using two reference waves having different wavelengths and propagation directions for the hologram recording. The principle of the method is exposed and experimental results concerning a 1.2μm m high test sample as well as a moving micro-mirror are presented. To the extent of our knowledge, this is the first time that real-time synthetic beat-wavelength digital holography measurements are reported.

© 2007 Optical Society of America

OCIS codes: (090.1760) Computer holography; (090.4220) Multiplex holography; (120.5050) Phase measurement; (180.3170 Interference microscopy)

References and links

1. J. W. Goodman and R. W. Lawrence, "Digital image formation from electronically detected holograms," Appl. Phys. Lett. **11**, 77–79 (1967).
2. U. Schnars and W. Jüptner, "Direct recording of holograms by a ccd target and numerical reconstruction," Appl. Opt. **33**, 179–181 (1994).
3. E. Cuche, F. Bevilacqua, and C. Depeursinge, "Digital holography for quantitative phase-contrast imaging," Opt. Lett. **24**, 291–293 (1999).
4. D. Gabor, "A new microscopic principle," Nature **161**, 777–778 (1948).

#81874 - $15.00 USD Received 6 Apr 2007; revised 16 May 2007; accepted 22 May 2007; published 29 May 2007

5. E. Cuche, P. Marquet, and C. Depeursinge, "Simultaneous amplitude-contrast and quantitative phase-contrast microscopy by numerical reconstruction of fresnel off-axis holograms," Appl. Opt. **38**, 6994–7001 (1999).
6. A. T. Forrester, W. E. Parkins, and E. Gerjuoy, "On the possibility of observing beat frequencies between lines in the visible spectrum," Phys. Rev. **72**, 728–728 (1947).
7. C. Polhemus, "Two-wavelength interferometry," Appl. Opt. **12**, 2071–2074 (1973).
8. F. Bien, M. Camac, H. J. Caulfield, and S. Ezekiel, "Absolute distance measurements by variable wavelength interferometry," Appl. Opt. **20**, 400–402 (1981).
9. R. Dändliker, R. Thalmann, and D. Prongué, "Two-wavelength laser interferometry using superheterodyne detection," Opt. Lett. **13**, 339–341 (1988).
10. B. P. Hildebrand and K. A. Haines, "Multiple-wavelength and multiple-source holography applied to contour generation," J. Opt. Soc. Am. **57**, 155–162 (1967).
11. J. S. Zelenka and J. R. Varner, "A new method for generating depth contours holographically," Appl. Opt. **7**, 2107–2110 (1968).
12. J. C. Wyant, "Testing aspherics using two-wavelength holography," Appl. Opt. **10**, 2113–2118 (1971).
13. C. Wagner, W. Osten, and S. Seebacher, "Direct shape measurement by digital wavefront reconstruction and multiwavelength contouring," Opt. Eng. **39**, 79–85 (2000).
14. J. Gass, A. Dakoff, and M. K. Kim, "Phase imaging without 2 pi ambiguity by multiwavelength digital holography," Opt. Lett. **28**, 1141–1143 (2003).
15. D. Parshall and M. Kim, "Digital holographic microscopy with dual wavelength phase unwrapping," Appl. Opt. **45**, 451–459 (2006).
16. T. Colomb, F. Montfort, J. Kühn, N. Aspert, E. Cuche, A. Marian, F. Charrière, S. Bourquin, P. Marquet, and C. Depeursinge, "Numerical parametric lens for shifting, magnification and complete aberration compensation in digital holographic microscopy," J. Opt. Soc. Am. A **23**, 3177–3190 (2006).
17. S. de Nicola, A. Finizio, G. Pierattini, D. Alfieri, S. Grilli, L. Sansone, and P. Ferraro, "Recovering correct phase information in multiwavelength digital holographic microscopy by compensation for chromatic aberrations," Opt. Lett. **30**, 2706–2708 (2005).
18. I. Yamaguchi, K. Yamamoto, G. A. Mills, and M. Yokota, "Image reconstruction only by phase data in phase-shifting digital holography," Appl. Opt. **45**, 975–983 (2006).
19. R. J. Mahon, J. A. Murphy, and W. Lanigan, "Digital holography at millimetre wavelengths," Opt. Commun. **260**, 469–473 (2006).
20. F. Zhang, G. Pedrini, and W. Osten, "Reconstruction algorithm for high-numerical-aperture holograms with diffraction-limited resolution," Opt. Lett. **31**, 1633–1635 (2006).
21. R. Onodera and Y. Ishii, "Two-wavelength interferometry that uses a fourier-transform method," Appl. Opt. **37**, 7988–7994 (1998).
22. A. W. Lohmann, "Reconstruction of vectorial wavefronts," Appl. Opt. **4**, 1667–1668 (1965).
23. E. N. Leith and J. Upatnieks, "Wavefront reconstruction with diffused illumination and three-dimensional objects," J. Opt. Soc. Am. **54**, 1295–1301 (1964).
24. E. N. Leith and J. Upatnieks, "Wavefront reconstruction with continuous-tone objects," J. Opt. Soc. Am. **53**, 1377–1381 (1963).
25. J. D. Armitage and A. W. Lohmann, "Theta modulation in optics," Appl. Opt. **4**, 400–403 (1965).
26. D. Beghuin, E. Cuche, P. Dahlgren, C. Depeursinge, G. Delacretaz, and R. P. Salathe, "Single acquisition polarisation imaging with digital holography," Electron. Lett. **35**, 2053–2055 (1999).
27. T. Colomb, P. Dahlgren, D. Beghuin, E. Cuche, P. Marquet, and C. Depeursinge, "Polarization imaging by use of digital holography," Appl. Opt. **41**, 27–37 (2002).
28. T. Colomb, E. Cuche, F. Montfort, P. Marquet, and C. Depeursinge, "Jones vector imaging by use of digital holography: simulation and experimentation," Opt. Commun. **231**, 137–147 (2004).
29. A. T. Saucedo, F. M. Santoyo, M. D. l. Torre-Ibarra, G. Pedrini, and W. Osten, "Endoscopic pulsed digital holography for 3d measurements," Opt. Lett. **14**, 1468–1475 (2006).
30. T. Saucedo A., F. M. Santoyo, M. D. l. T. Ibarra, G. Pedrini, and W. Osten, "Simultaneous two-dimensional endoscopic pulsed digital holography for evaluation of dynamic displacements," Appl. Opt. **45**, 4534–4539 (2006).
31. E. Cuche, P. Marquet, and C. Depeursinge, "Spatial filtering for zero-order and twin-image elimination in digital off-axis holography," Appl. Opt. **39**, 4070–4075 (2000).
32. T. Colomb, E. Cuche, F. Charrière, J. Kühn, N. Aspert, F. Montfort, P. Marquet, and C. Depeursinge, "Automatic procedure for aberration compensation in digital holographic microscopy and applications to specimen shape compensation," Appl. Opt. **45**, 851–863 (2006).
33. P. de Groot and S. Kishner, "Synthetic wavelength stabilization for two-color laser-diode interferometry," Appl. Opt. **30**, 4026–4033 (1991).
34. Y. Emery, E. Cuche, F. Marquet, N. Aspert, P. Marquet, J. Kühn, M. Botkine, T. Colomb, F. Montfort, F. Charrière, C. Depeursinge, P. Debergh, and R. Conde, "Digital holographic microscopy (DHM) for metrology and dynamic characterization of MEMS and MOEMS", Proc. SPIE **6186**, N1860–N1860 (2006).

#81874 - $15.00 USD Received 6 Apr 2007; revised 16 May 2007; accepted 22 May 2007; published 29 May 2007
(C) 2007 OSA

1. Introduction

The technique of digital holography has experienced substantial developments in the past years [1–3] as charge coupled device (CCD) and digital image processing technologies progressed. In a way similar to classical holography [4], it enables to retrieve the original object wavefront - in amplitude and phase - but with the difference that quantitative and accurate phase information can be obtained thanks to the numerical reconstruction process of the hologram. Digital holographic microscopy (DHM) provides reconstructed images with a diffraction-limited lateral resolution down to a few hundreds of nanometers depending on the microscope objective (MO) numerical aperture (NA). On the other hand, the axial resolution is less than $\lambda/150$ due to the interferometric nature of the method [5]. However, the very sensitive information provided by the phase has the downside to be only defined modulo 2π. Consequently, optical path lengths (OPL) larger than one time the wavelength cannot be unequivocally measured, resulting in a phase ambiguity. In a majority of situations, phase unwrapping algorithms can be used to retrieve the true OPL map of the sample, but high aspect-ratio objects, such as specimens with step height, or high roughness surface, as well as noisy experimental conditions can make such algorithms failing. In addition, such unwrapping methods are often time-consuming making them inadequate for real-time measurements.

Already in 1947, Forrester *et al.* [6] proposed to combine two illumination wavelengths to create a so-called beat-wavelength much larger than the original ones, in the microns- or even millimeters-range. By obtaining the phase or contour map of the sample with this beat-wavelength, the phase ambiguity at single wavelength is removed and the vertical measurement range is greatly extended. This has been successfully applied in interferometry [7–9] and holography [10–12] since the early 70'.

Dual-wavelength digital holography was first introduced by Wagner *et al.* [13] by subtraction of two reconstructed phase maps obtained with a scanning dye laser to perform a millimeter contouring of the object. Recently, Kim's group proposed a similar technique within the framework of DHM in order to remove the phase ambiguity of digitally-propagated wavefronts [14, 15]. First, a synthetic phase map is computed as the difference between the two different wavelengths phase maps. Then, integer multiples of one of the wavelengths, obtained from the synthetic phase map, is added to the same wavelength phase map. Such different wavelengths phase maps subtraction requires achromatic setups, otherwise numerical image resizing is needed, as explained in Refs. [16] and [17]. Instead of using two different laser sources, it is also possible to use the mode-hope of a laser diode to change the wavelength [18] or to generate a millimeter-range wavelength with a terahertz source [19, 20].

However, all the published two-wavelengths digital holography methods require a sequential approach to record the information from both sources, with repeated acquisitions for each wavelength. This prevents real-time dual-wavelength measurements because at least two camera acquisitions are needed. For phase-shifting techniques multiple exposures, typically three, are needed to retrieve the phase map for a single wavelength. Consequently, monitoring moving samples or measuring in presence of vibrations are precluded. A solution was proposed by Onodera *et al.* in Ref. [21] for Fourier interferometry. A single interferogram is recorded with two different wavelengths having the same propagation directions. When analyzing the hologram in its Fourier components, two slightly different spatial carrier frequencies appear, due to the wavelength difference (fringe density change), that can be separately filtered and centered in the origin of the Fourier plane. Then, the application of an inverse-Fourier transform provides two phase maps that are processed to obtain the synthetic phase distribution. Nevertheless, the technique is only applicable to in-focus images, as no wavefront propagation occurs. Furthermore the object spectrum should not contain too high spatial frequencies to avoid overlapping, since the carrier frequency separation in the spectrum is very small with identical propagation

#81874 - $15.00 USD Received 6 Apr 2007; revised 16 May 2007; accepted 22 May 2007; published 29 May 2007
(C) 2007 OSA

directions for the reference waves.

In this paper, we demonstrate that multi-reference waves DHM is a solution to overcome these drawbacks. The original idea of multiple reference waves was developed in classical holography by Lohmann in 1965 in Ref. [22] where a spatial multiplexing of wavelengths (also presented in Refs. [23–25]) and of polarization is proposed. Then, this idea was applied in digital holography for polarization imaging by spatial multiplexing with two different orthogonally polarized reference waves [26–28], and for multiple illumination angles in endoscopic digital holography [29,30]. Here, we show that a dual-wavelength spatial multiplexing in digital holography enables single-acquisition beat-wavelength measurements and provides an ideal solution to compensate for chromatic aberrations. Indeed, digital reconstruction distances can be adjusted separately for each wavelength, providing in-focus images even if the specimen moves out-of-focus or in case of slight chromatic aberrations. Furthermore, for stronger chromatic aberrations, this method is fully compatible with digital processing techniques such as digital optics [16] or hologram padding [17], that allow numerical resizing for numerical propagations, achieved respectively with convolution or Fresnel-Kirschoff formalism, resulting in a perfect superposition of the two phase distributions. Most importantly, obtaining complex wavefront information for both wavelengths, by recording a single hologram, permits the computation of the phase difference between each wavefront for each acquisition, and thus provides real time beat-wavelength imaging.

2. Principle

Let us take the example of a hologram acquired by a digital camera, with two collinear object beams $\boldsymbol{O}_1$ and $\boldsymbol{O}_2$ at two different wavelengths λ_1 and λ_2 that interfere with two reference beams $\boldsymbol{R}_1$ and $\boldsymbol{R}_2$, emitted by the same pair of laser sources, in a off-axis configuration (slight angle between object and reference beams). The intensity pattern, which results from an incoherent addition of both interferograms at λ_1 and λ_2, can be expressed as

$$I_H(x,y) = |\boldsymbol{R}_1|^2 + |\boldsymbol{O}_1|^2 + |\boldsymbol{R}_2|^2 + |\boldsymbol{O}_2|^2 + \boldsymbol{R}_1\boldsymbol{O}_1^* + \boldsymbol{R}_1^*\boldsymbol{O}_1 + \boldsymbol{R}_2\boldsymbol{O}_2^* + \boldsymbol{R}_2^*\boldsymbol{O}_2, \tag{1}$$

with I_H being the hologram intensity; x, y the coordinates in the camera plane, and * denoting the complex conjugate.

The first four terms in Eq. 1 correspond to the zero order of diffraction, and can be easily filtered in the Fourier domain [31]. The last four terms correspond to the interference of the object wavefronts $\boldsymbol{O}_i$ (the virtual images), or their conjugate $\boldsymbol{O}_i^*$ (the real images), with the reference waves. These interferences appear as fringes at carrier spatial frequencies on the hologram. With $\boldsymbol{O}_i$ collinear on the optical axis, these carrier frequencies are dependent on the k-vectors of $\boldsymbol{R}_1$ and $\boldsymbol{R}_2$. Considering different incident angles for the two references waves, especially the configuration where their k-vector projections on the CCD plane are orthogonal, each interference term occupies different position in the Fourier plane. Providing that there is no overlap between interference terms, a condition which imposes restrictions regarding the spatial frequency content of the object spectrum, it is therefore straightforward to isolate each frequency component by spatial filtering [31]. Then it is possible to numerically propagate in a separate manner the two associated wavefronts. Such a procedure is similar to the one of polarization imaging with digital holography [26–28] or multiple angles endoscopic digital holography [29, 30]. Practically, the two different spatial filters allow to treat the two interferences terms $\boldsymbol{R}_1^*\boldsymbol{O}_1$ and $\boldsymbol{R}_2^*\boldsymbol{O}_2$ independently.

Writing these two filtered holograms as $I_{H,1}^F$ for $\boldsymbol{R}_1^*\boldsymbol{O}_1$ and and $I_{H,2}^F$ for $\boldsymbol{R}_2^*\boldsymbol{O}_2$ and and by using the convolution formulation, we obtain the following expression for the Fresnel propagation:

#81874 - $15.00 USD Received 6 Apr 2007; revised 16 May 2007; accepted 22 May 2007; published 29 May 2007
(C) 2007 OSA

$$\Psi_{\mathrm{CF,i}}(m,n) = \Gamma_i^I(m,n) \cdot \frac{\exp(i2\pi d_i/\lambda_i)}{i\lambda_i d_i} \cdot \mathrm{FFT}^{-1}\left\{ \mathrm{FFT}\left[\Gamma_i^H(k,l) I_{H,i}^F(k,l)\right] \cdot \exp\left\{ -i\pi\lambda_i d_i \left[\left(\frac{k}{N\Delta x}\right)^2 + \left(\frac{l}{N\Delta y}\right)^2 \right] \right\} \right\}, \quad (2)$$

where $\Psi_{\mathrm{CF,i}}$ is the reconstructed wavefront for wavelength λ_i in the convolution formulation, Γ_i^I and Γ_i^H are digital phase masks (DPM) in the image plane and in the hologram plane respectively, used to compensate for aberrations (see Ref. [32] for details), d_i is the propagation distance for wavelength λ_i, FFT is the Fast Fourier Transform operator, (k, l) and (m, n) are the couple of integers so that $(-N/2 < k,l,m,n \leq N/2)$ representing coordinates in the hologram plane, respectively the reconstruction plane, NxN is the number of pixels of the CCD camera and Δx and Δy are the pixel sizes.

The formulation of Eq. 2 enables to propagate each wavefront $\Psi_{\mathrm{CF,i}}$ in an independent manner: the DPMs can be adapted to compensate for each wavefront aberrations and the propagation distances d_i can be adjusted differently to compensate for slight chromatic aberrations or specimen displacement with respect to the working distance of the MO. Let us mention that the DPM could also be used as digital magnification lenses to resize the images in the case of stronger chromatic aberrations [16]. The parallel propagations with 512x512 pixels holograms are achieved with a frame rate of about 7 frames per second with a standard dual-core PC at 2 GHz (roughly half the standard reconstruction rate). A a-posteriori hologram stack reconstruction can also be performed and is only limited by the acquisition rate of the CCD camera (here 25 frames per second). The reconstructed complex wavefronts $\boldsymbol{O}_1$ and $\boldsymbol{O}_2$ in the reconstruction plane contain information both in amplitude and in phase, providing a nanometer-scale resolution in the vertical axis but suffering from phase ambiguity for OPLs larger than the wavelength. The calculation of $\boldsymbol{O}_1\boldsymbol{O}_2^*$ in the reconstruction plane allows to obtain the following expression for the synthetic wavelength phase:

$$\Phi = \arg(\boldsymbol{O}_1\boldsymbol{O}_2^*) = \phi_1 - \phi_2 = 2\pi\frac{x}{\lambda_1} - 2\pi\frac{x}{\lambda_2} = 2\pi x\left(\frac{\lambda_2-\lambda_1}{\lambda_1\lambda_2}\right) = 2\pi\frac{x}{\Lambda}, \quad (3)$$

where x is the OPL (twice the topography in reflection, for an homogeneous sample in air), ϕ_i the reconstructed phase for the wavelength λ_i and Λ is the synthetic beat wavelength defined as:

$$\Lambda = \frac{\lambda_1\lambda_2}{\lambda_2-\lambda_1}. \quad (4)$$

This beat wavelength is much larger than the original couple of wavelengths, the smaller the difference (λ_2-λ_1), the larger the synthetic wavelength, typically within the range of micrometers to millimeters. The corresponding synthetic phase obtained with Eq. 3 enables to resolve much higher structures by removing the phase ambiguity in the range of the beat wavelength Λ, thus greatly increasing the range for the phase measurement.

Despite this advantage, it should be noticed that the laser sources wavelengths stability is a top-priority issue for direct synthetic wavelength imaging [33]. Indeed, any variations in wavelength is amplified when the beat wavelength phase map is computed according to Eqs. 3 and 4, and the noise on the phase ϕ_1 or ϕ_2 is also amplified when converted in topography due to the important value of Λ. Thus, high stability laser sources are required as well as careful setup design to minimize noise sources and use of low temporal coherence sources to avoid parasitic interferences. Nevertheless, methods to keep the single-wavelength precision by using the synthetic phase only for phase ambiguity removal, like the ones presented in Refs. [14] and [15],

#81874 - $15.00 USD Received 6 Apr 2007; revised 16 May 2007; accepted 22 May 2007; published 29 May 2007
(C) 2007 OSA

can potentially nullify this effect and render the technique more forgiving regarding wavelength stability.

At this point, if we compute the phase difference Φ (Eq. 3) for each reconstructed hologram, it becomes possible to measure, in real time, the object under investigation as if a source of wavelength Λ were used. In this paper, the methods is demonstrated with live measurements on samples up to 2μm high with a synthetic wavelength of $\Lambda = 6.4\mu$m.

3. Experimental configuration

The setup used for real-time two-wavelengths DHM is depicted in Fig. 1. The laser sources are two temperature-stabilized semiconductor laser diodes at $\lambda_1 = 679.57$nm and $\lambda_2 = 759.91$nm, yielding $\Lambda = 6.428\mu$m for the synthetic beat wavelength. The diodes were tested for wavelength stability with a wavemeter and showed a wavelength deviation smaller than 10pm over 8h. The corresponding measurement error for a 3μm high step (nearly $\Lambda/2$), caused by an unwanted change of Λ, is less than $1\mathring{A}$. The diodes also emits a low coherence (coherence length about 0.3mm) linearly polarized light.

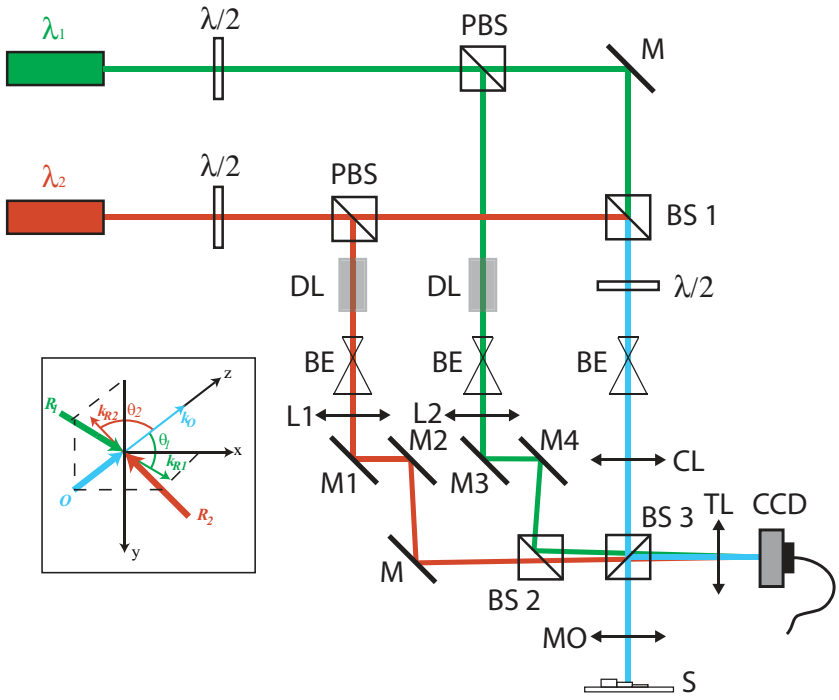

Fig. 1. Two-wavelengths DHM setup. $\lambda/2$: half-waveplate, M: mirrors, PBS: polarizing beamsplitter, BS: non-polarizing beamsplitter, DL: delay line, BE: beam-expander, L: lens, CL: condenser lens, MO: x3 achromatic microscope objective, 0.1 NA, S: specimen, TL: tube lens; Inset: 3D distribution of the incident waves propagation directions upon the CCD plane, k_{R1} and k_{R2} are the propagation direction vector of the reference waves $\boldsymbol{R}_1$ for wavelength λ_1 and $\boldsymbol{R}_2$ for λ_2.

The principle of the setup is to separate both wavelengths beams in different reference arms, while aligning and combining them in an achromatic object arm. After reflection on the sample, both collinear object wavefronts are collected by the MO (infinity-corrected), and the object images are formed by the tube lens (focal 150mm) about 5cm behind the CCD plane. A low

#81874 - $15.00 USD Received 6 Apr 2007; revised 16 May 2007; accepted 22 May 2007; published 29 May 2007
(C) 2007 OSA

magnification x3 MO, with a NA of 0.1, is used in the present case to achieve large field-of-view (FOV), 1x1mm^2 with 512x512 pixels, and a large depth-of-field of more than 50μm. We can mention that there is no limitation regarding the use of higher magnification. The CCD camera is a standard 8 bits black and white CCD camera with 6.45μm pixel size. Each reference arm comprise a delay line (DL) adjusted to match the optical path length of its respective object counterparts, in order to create an interference on the CCD for both wavelengths. By tilting the pair of mirrors M1 and M2 for the first wavelength reference beam, respectively M3 and M4 for the second one, one can finely tune each k-vector incident upon the CCD camera. In other words, each wavelength interferograms fringes can be independently tuned both in spatial frequency and orientation.

The ideal configuration for dual-wavelength DHM is the one depicted in the inset of Fig. 1, with orthogonal spatial frequencies for each wavelength interferogram, because it ensures an optimum repartition of the interference terms in the hologram Fourier domain, minimizing overlaps. A typical dual-wavelength hologram and its Fourier spectrum are represented in Fig. 2, with the real and virtual images components for each wavelength interferogram and the orthogonal fringes regimes.

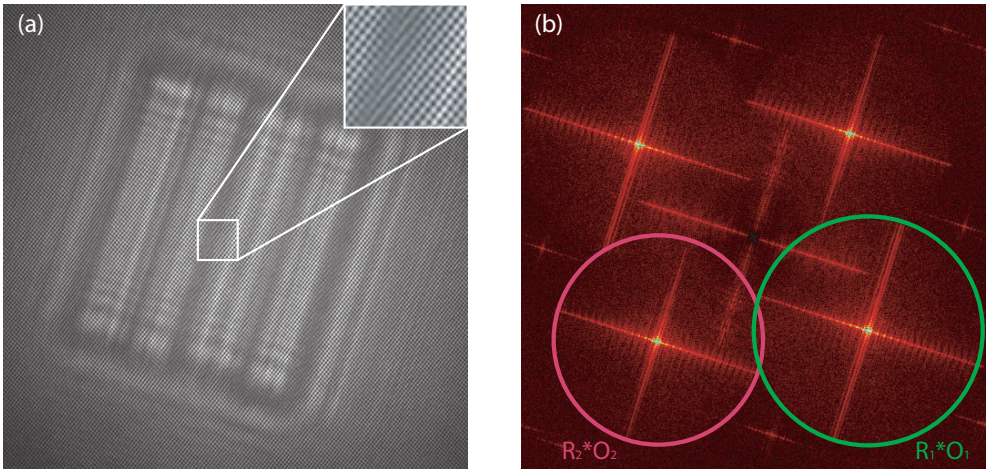

Fig. 2. (a) Two-wavelengths hologram with the inset representing a zoom on the central fringes, where the orthogonal spatial frequencies can be seen; (b) Fourier-spectrum of (a) (the zero order is filtered to enhance visibility), where the virtual images for each wavelength are easily separately spatial-filtered (red = 760nm, green = 680nm)

As can be seen in Fig. 2, the orthogonal repartition of the fringes spatial frequencies enables to filter (select) separately the spatial frequencies of each wavelength in the Fourier spectrum of the hologram. In other words, the real image components $\boldsymbol{R}_i\boldsymbol{O}_i^*$, or the virtual image components $\boldsymbol{R}_i^*\boldsymbol{O}_i$, or any other set of interference terms, can be selected independently as depicted in Fig. 2(b), and this procedure is rendered easier by the clearly visible cut-off frequency of the MO (colored circles in Fig. 2(b). This experimental configuration for recording holograms is very similar to the one in Ref. [27,28] and permits to encode both wavefronts with only a single acquisition thanks to orthogonal carrier frequencies. It can also be noted that the circle is a bit larger at 680nm, indicating a slightly higher cut-off frequency at this wavelength. A transverse resolution of 4.4μm has been measured with a USAF 1950 resolution test target and the system is diffraction-limited according to the NA of the MO.

It is however important to mention that there is a trade-off here, in the sense that by using off-axis holography it is indeed possible to separate the terms in the spatial frequency domain,

#81874 - $15.00 USD Received 6 Apr 2007; revised 16 May 2007; accepted 22 May 2007; published 29 May 2007
(C) 2007 OSA

thus enabling single-acquisition imaging, but at the cost of a reduction by a factor two of the field of view compared to in-line holography, where the full sampling efficiency of the CCD can be exploited. That is, one need to use a higher magnification factor in off-axis holography than with in-line holography to prevent resolution loss due to the use of only half the CCD sampling capability.

Once each wavelength interference term, here the two virtual images components, is spatially-filtered, one can use Eq. 2 to reconstruct and propagate each wavefront in the convolution formalism. By correcting for aberrations in the hologram plane before the propagation, especially the tilt, the reconstructed images are naturally centered [16]. This perfect superposition and the achromatic design of the object arm of the setup, allow for an accurate subtraction of the wavefronts in the image plane. The reconstruction distances in the experimental configuration of Fig. 1 are $d_1 = 50$mm for $\lambda_1 = 680$nm and $d_2 = 50.5$mm for $\lambda_2 = 760$nm and they correspond to the distances between the image planes and the CCD plane. As the reconstruction distances difference is very small due to the achromatic conditions, the magnification difference can be considered negligible and the superposition conditions are fulfilled.

For this setup, a high quality mirror has permitted to evaluate an experimental noise of about 2 degrees of phase spatial standard deviation over the whole field-of-view in phase for each wavefront. It should be noted that this spatial standard deviation value is the same as for single-wavelength DHM. This is valid for a single hologram reconstruction with contribution of both the setup noise and the shot noise, at the instant of acquisition, which corresponds to a speckle noise for this frame. The time-dependant part of the noise, mainly shot noise for instance, can be reduced by temporal averaging methods if necessary. When considering the synthetic beat phase Φ, the spatial standard deviation raises to about 3 degrees. In terms of axial topographic resolution, this corresponds to about 2nm precision for monochromatic phases, and 27nm for the beat-wavelength phase precision, which is a consequence of the noise amplification phenomena. The standard deviation value for the synthetic phase is directly related to the property that the variance of the sum (or difference) of two Gaussian-noise distributions is the sum of the individual variances: we have precisely here a $\sqrt{2}$ amplification for the standard deviation when considering the phase difference of two signals with quasi-identical standard deviations. Let us once again point out that the same method as in Refs. [14] and [15] could be used to keep the single-wavelength precision by solving the phase ambiguity with the synthetic phase map, and then adding integer multiple of one of the two wavelengths to the corresponding single-wavelength phase map. For such solutions to work, the noise level should be kept below $\lambda_i/4\Lambda$ [14], which is largely the case in our experimental configuration, but this condition may not be always satisfied for e.g. noisy data or high-range beat wavelengths.

4. Results

To validate the technique, we have choosen a purely-reflective object with abrupt steps of more than half a visible-range wavelength in height. Such a specimen cannot be observed with monochromatic DHM because the phase ambiguity is nearly impossible to solve with the help of unwrapping algorithms, due to the steep transitions compared to the lateral resolution. The object is a micro-structured SiO_2 staircase on a Si wafer with a gold coating to ensure a perfect reflectivity. It is made of five steps with the following height values: 375, 525, 975, 1200, 1275nm inducing up to 2.5μm in term of OPL, which represents about four times a typical red-range wavelength and out of range of classical single-wavelength DHM. A schematic of this test-object and experimental reconstruction images of this sample from the hologram of Fig. 2 with the two-wavelength setup of Fig. 1 are presented in Fig. 3

#81874 - $15.00 USD Received 6 Apr 2007; revised 16 May 2007; accepted 22 May 2007; published 29 May 2007
(C) 2007 OSA

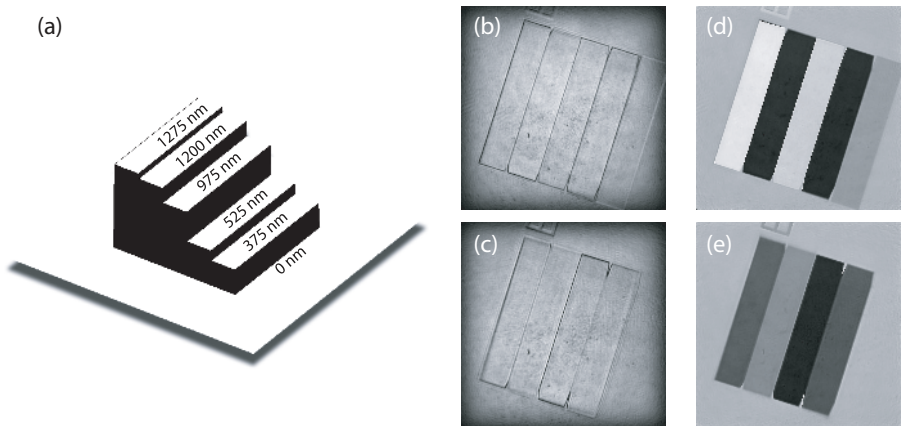

Fig. 3. (a) Schematic of the investigated staircase test-sample; (b,c) amplitude and (d,e) phase of respectively the reconstructed wavefront $\boldsymbol{O}_1$ ($\lambda_1 = 680$nm, $d_1 = 5$cm) and $\boldsymbol{O}_2$ ($\lambda_2 = 760$nm, $d_2 = 5.05$cm) obtained from the same hologram presented in Fig. 2 (grayscale: black = -180, white = +180 for the phase; field-of-view: 1x1mm^2)

The two reconstructed quantitative phase-contrast images of the object in Fig. 3(d,e) obtained from the same hologram recording (Fig. 2) illustrate the phase ambiguity for single-wavelength imaging: the smallest step of 375nm is invisible in Fig. 3(e) because it corresponds to an OPL of 750nm, which is nearly the value of $\lambda_2 = 760$nm. Unwrapping algorithms are clearly useless for such micro-structures investigation. As we have recorded both wavefronts with the same hologram acquisition, the computation of the phase difference between Figs. 3(d) and 3(e) can be achieved according to Eq. 3. After inversion of the sign of the phase to render a topographic map (i.e. a conjugated phase map), as will be done for all synthetic phase-maps further on, we obtain the $\Lambda = 6.428\mu$m synthetic wavelength conjugated phase distribution presented in Fig. 4.

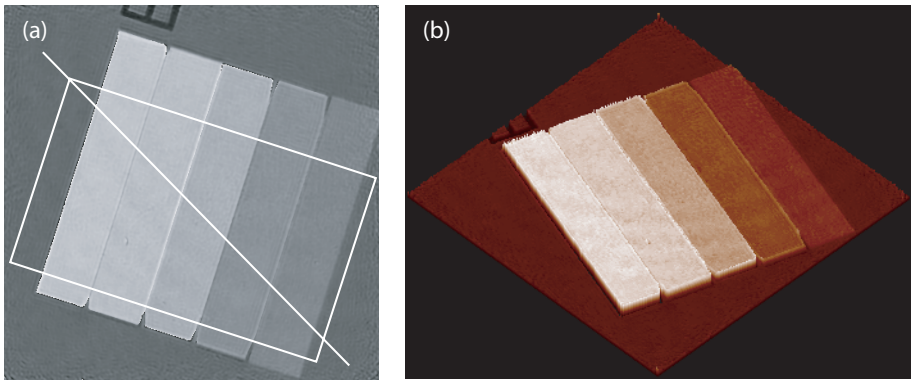

Fig. 4. Single-hologram beat-wavelength conjugated phase map of the sample of Fig. 3 at $\Lambda = 6.428\mu$m (grayscale: black = -180, white = +180). (a) Synthetic phase-contrast image of the Si staircase sample at $\Lambda = 6.428\mu$m; (b) 3D perspective of (a).

#81874 - $15.00 USD Received 6 Apr 2007; revised 16 May 2007; accepted 22 May 2007; published 29 May 2007
(C) 2007 OSA

The measurement of the object with a beat-wavelength of $\Lambda = 6.428\mu$m straightforwardly provides a phase jumps-free result and a real 3D-topography of this up to 1.275μm high specimen as illustrated in Fig. 4(b). To assess the method, quantitative profiles measurements on the synthetic map of Fig. 4 are given in Fig. 5 and compared with results obtained with a white light interferometer.

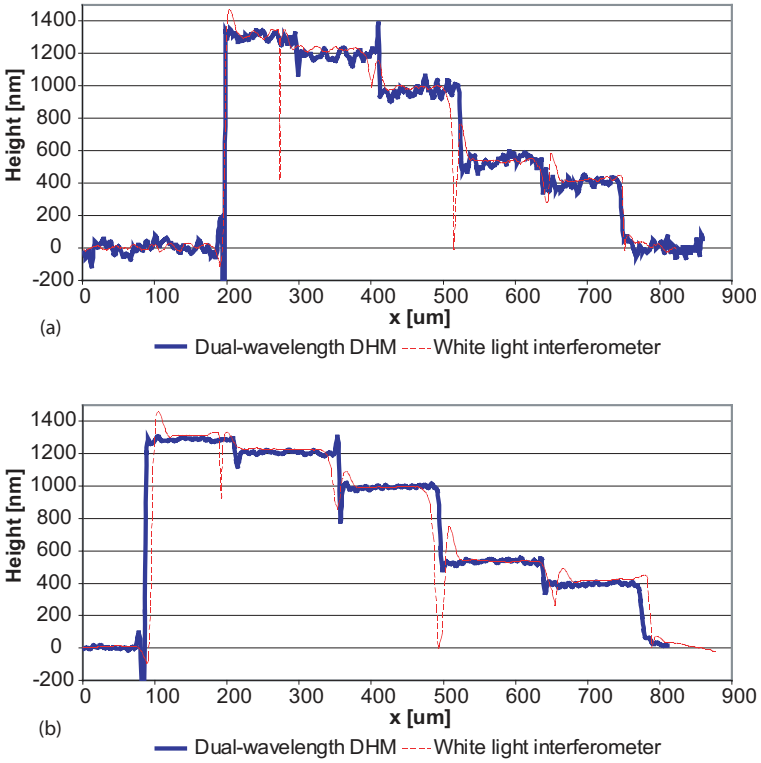

Fig. 5. (a) Profile line taken along the white line in Fig. 4(a) superposed with a profile obtained with a commercial white light interferometer; (b) spatial average of about 100 profiles taken perpendicular to the small edge of the white rectangle defined in Fig. 4(a) compared with the average profile measured with the white light interferometer.

As can be seen in Fig. 5, the quantitative experimental results with two-wavelengths DHM are in agreement with the white-light interferometry results and within the manufacturing error of 2% of the theoretical topographic values. Despite the standard deviation of the beat-wavelength phase of ~ 27nm, it is still easily possible to discriminate the 1.2μm and 1.275μm steps. Furthermore, the precision can be enhanced by spatially averaging 100 profiles as in Fig. 5(b), where the measure seems even more accurate than with the white light interferometer. This spatial averaging is done for a single reconstruction, and it applies on both the setup and the speckle noise (shot noise at the instant of acquisition).

Nevertheless, the requirement to record only a single digital hologram is the true added-value of the method. Thus, to demonstrate the real-time capability of the technique, the sample is manually translated in one direction during 40s along different sizes of SiO_2 staircases with the same heights staircases, and the sequence is recorded at the maximum frame rate of 25 images/s (1'000 acquisitions). Results illustrating the real-time synthetic wavelength phase maps are presented as multimedia movies in Fig. 6.

#81874 - $15.00 USD Received 6 Apr 2007; revised 16 May 2007; accepted 22 May 2007; published 29 May 2007
(C) 2007 OSA

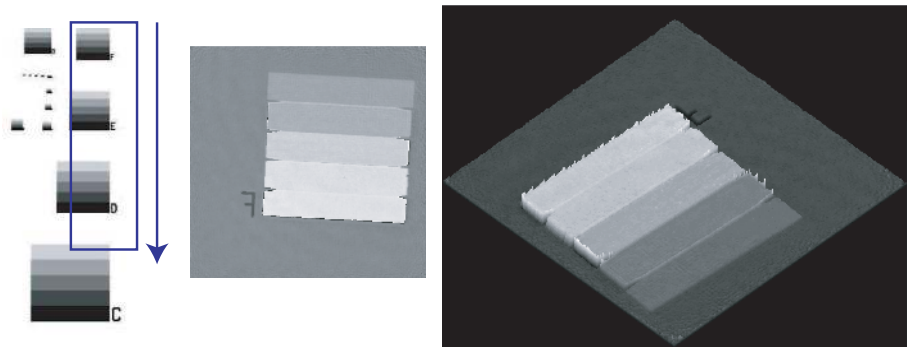

Fig. 6. Real-time beat-wavelength phase imaging by DHM. (a) Scanning orientation map on the micro-structures array; (b) 40s movie of the $\Lambda = 6.428\mu$m phase-contrast image at 25 images/s (test_target_ph.mov, 2.62 MB); (c) 3D perspective view of (b) (test_target_3D.mov, 2.6 MB)

The real-time capability illustrated above is especially useful for moving samples measurements on a conveyor belt, in a similar way like with the translation in Fig. 6, or moving MEMS/MOEMS parts monitoring either in real-time or in stroboscopic mode [34]. To illustrate this advantage of the method, Fig. 7 presents a 6 seconds movie (25 frames/second, 150 acquisitions) of the phase reconstruction of a electrically-actuated 4x4mm ^{2} micro-mirror oscillating at 1Hz, for a single wavelength [Fig. 7(a)] and for synthetic wavelength [Fig. 7(b,c)].

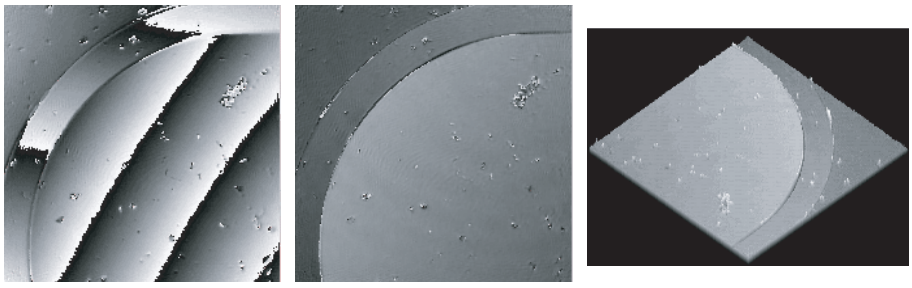

Fig. 7. Dual-wavelength phase measurements on a moving micro-mirror oscillating at 1Hz during 6s at 25 frames/s. (grayscale: black = -180, white = +180; field-of-view: 1x1mm^2) (a) Phase movie at the wavelength $\lambda_1 = 680$nm (mems_680nm.mov, 2.79 MB); (b) Phase movie at the beat wavelength $\Lambda = 6.428\mu$m (mems_beat_wav.mov, 1.72 MB); (c) 3-D perspective of (b) (mems_3D.mov, 2.6 MB

Figure 7 shows clearly the efficiency of the synthetic wavelength imaging, free of phase jumps, for such moving micro-parts investigation. Figure 8 demonstrates the usefulness of dual-wavelength real-time DHM and its ideal application for MEMS/MOEMS investigation by providing quantitative height measurements expressed by a profile line taken through the whole field of view (FOV) during half-a-period of oscillation (0.5s). In addition the dual-wavelength method is more robust than a time unwrapping that could be applied for a single wavelength. Indeed, if the mirror raises more than a few hundred of nanometers ($\lambda_i/2$) between two acquisition (as for example between 0.12 and 0.25 second in Fig. 8), a temporal phase unwrapping method may fail.

#81874 - $15.00 USD Received 6 Apr 2007; revised 16 May 2007; accepted 22 May 2007; published 29 May 2007
(C) 2007 OSA

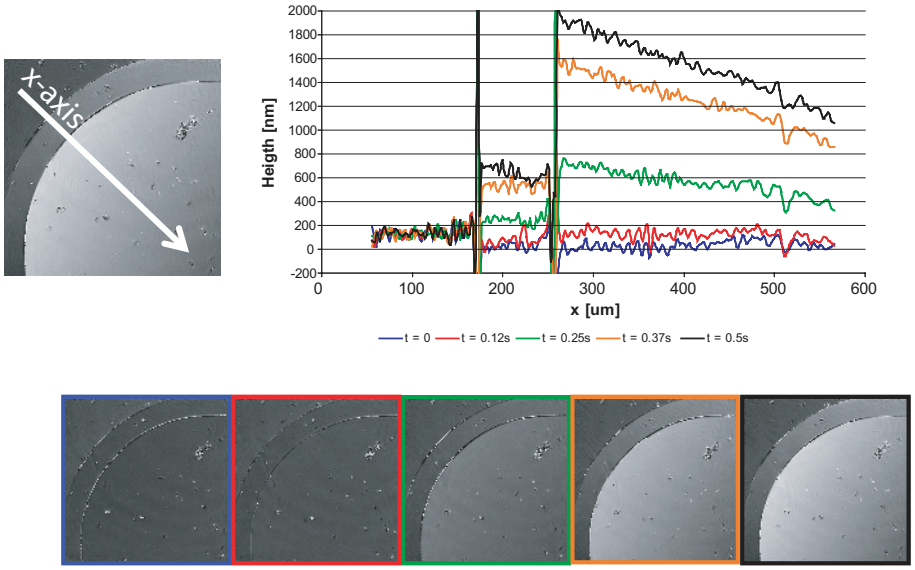

Fig. 8. Half-a-period monitoring of micro-mirror movements at the synthetic wavelength $\Lambda = 6.428\mu$m

5. Conclusion

We have presented a method to achieve real-time dual-wavelength digital holographic microscopy with a single hologram acquisition. The principle is based on a spatial multiplexing of the hologram by incoherent addition of single-wavelength interferograms, each having different propagations directions for the reference waves. The property of off-axis digital holography to separately extract the spatial frequencies associated to each wavefront, and to propagate them in parallel, permits to reconstruct the synthetic wavelength phase distribution of a reflective object with a single acquisition. Consequently, the dynamic range of phase measurements is increased and the phase ambiguity of single-wavelength imaging is removed. Results obtained with our method on a 1.2μm high test-target imaged at 25 frames/s with a 6.4μm synthetic wavelength are in good agreement with white light interferometer measurements. Further on, this method allows for observing fast phenomena and the dynamic performance has been illustrated with a 1Hz oscillating micro-mirror monitoring at video frequency.

The development of the technology has been supported by Swiss government through CTI grants TopNano 21 #6101.3 and NanoMicro #6606.2 and #7152.1. The author thanks the people at Lyncee Tec SA (www.lynceetec.com) for their collaboration and the fruitful discussions.

#81874 - $15.00 USD Received 6 Apr 2007; revised 16 May 2007; accepted 22 May 2007; published 29 May 2007
(C) 2007 OSA